Theory of exciton-polaron complexes in pulsed electrically detected magnetic resonance

T. L. Keevers,[1,*] W. J. Baker,[1,2] and D. R. McCamey[1]

[1]*School of Physics, UNSW Australia, Sydney NSW 2052, Australia*

[2]*Centre for Quantum Computation and Communication Technology, UNSW Australia, Sydney NSW 2052, Australia*

(Received 4 February 2015; revised manuscript received 21 April 2015; published 15 May 2015)

Several microscopic pathways have been proposed to explain the large magnetic effects observed in organic semiconductors; however, it is difficult to identify and characterize the microscopic process which actually influences the overall magnetic field response in a particular instance. Pulsed electrically detected magnetic resonance provides an ideal platform for this task as it intrinsically monitors the charge carriers of interest and provides dynamical information which is inaccessible through conventional magnetoconductance measurements. Here we develop a general time-domain theory to describe the spin-dependent recombination of exciton-polaron complexes following the coherent manipulation of paramagnetic centers through electron paramagnetic resonance. A general Hamiltonian is treated, and it is shown that the transition frequencies and resonance positions of the exciton-polaron complex can be used to estimate interspecies coupling. This work also provides a general formalism for analyzing multipulse experiments which can be used to extract relaxation and transport rates.

DOI: 10.1103/PhysRevB.91.205206 PACS number(s): 71.35.−y

I. INTRODUCTION

Organic devices with nonmagnetic electrodes can display large magnetoresistances at room temperature [1]: Magnetic fields of 10 mT or less are sufficient to induce large changes in sample conductivity [2], with reports of changes exceeding 2000% in one-dimensional wires [3]. There is interest in harnessing these field-induced effects to enhance technologies including solar cells [4], organic light-emitting diodes [5], and cheap magnetic sensors [6]. This requires sophisticated methods for characterizing and engineering the underlying spin processes.

Several detailed models [7–9] have been developed to explain the ubiquitous magnetoconductance effects observed in organic devices. In recent years there has been significant progress in distinguishing potential spin processes through line shape and voltage fingerprints [10]; these types of quasistatic measurements and models are fundamentally limited: dynamical rates and energetic couplings are obscured by the effects of spin ensemble averaging and the intrinsically incoherent nature of the measurement. Coherent spectroscopic techniques, such as pulsed electron paramagnetic resonance (pEPR), provide a way to independently identify and quantify the underlying physical processes because they allow subensemble of spins to be selectively addressed and manipulated within the spin coherence time [11].

Pulsed electrically detected magnetic resonance [12] (pEDMR) provides a strong spectroscopic probe with which to investigate these processes, as different spin processes can readily be disentangled [11,13] and their impact on device operation directly observed from the transient dynamics. Pulsed methods are able to access coherent time-domain information and by adjusting the applied pulse sequence different aspects of the spin ensemble can be probed, allowing a holistic picture of the spin physics to be developed and rigorously tested [14]. Past studies have primarily focused on pristine poly[2-methoxy-5-(2-ethylhexyloxy)-1,4-phenylenevinylene] (MEH-PPV) devices in which polaron pairs are the dominant spin-reaction pathway, and a detailed picture of the relevant energy and time scales in these devices has been developed [15,16]. Dissociation, recombination, and intersystem crossing rates have been characterized [17,18], as well as the strength of the electron-nuclear coupling [19] and spin-spin interactions within the pair [18]. Recent improvements in pEDMR measurement methods have substantially improved signal to noise [20], and a variety of standard one and two-dimensional experiments with pEPR [14] are now technically feasible. In contrast, energy and time scales cannot be effectively separated in quasistatic magnetoconductance measurements; Ultrasmall field effects are consistent with either a weak exchange interaction [21] or slow carrier hopping [22]. Differentiation between these two scenarios is possible with pulsed measurements [15,16]; however, no comparable fingerprint is known for the static case.

An extensive body of literature has been developed for describing the time-domain response of polaron pairs in magnetic resonance [23–25], while comparatively little is known in relation to three-particle processes. These are expected to include triplet-exciton polaron quenching or the dynamics of a bipolaron stabilized by a counterion in organic systems [26]. Other three-particle processes also include spin-dependent Auger recombination in nanocrystals [27], trion states in silicon [28], and electrons interacting with a common nuclear bath [29].

In this work we develop a general formalism for describing the spin-dependent response of three-particle complexes in pEDMR, thus providing the theoretical foundations for the quantitative characterization of the time and energy scales present in these systems.

There are a number of different mechanisms invoked in the literature to describe triplet-exciton polaron quenching (TEP). For instance, Desai *et al.* [8] described a mechanism in which free polarons scatter from trapped triplet excitons, causing the excitons to cross from the triplet to singlet manifold,

$$T_{1,0,-1} + D_{\pm 1/2} \leftrightarrow (T_{1,0,-1} \ldots D_{\pm 1/2}) \rightarrow D_{\pm 1/2} + S^{*}, \quad (1)$$

*t.keevers@student.unsw.edu.au

where T_i is an excited triplet exciton with a spin projection of -1, 0, or $+1$, D_i is a free charge carrier with a spin projection $m_s = i$, S is a singlet exciton, and $*$ denotes an excited state. The reaction rate was assumed to be spin dependent, although no microscopic mechanism was provided. In contrast, Koopmans and co-workers describe a quenching process which depends on the overall quartet or doublet content of the pair and may increase or decrease the polaron's mobility [22]. Other implementations include a site-blocking mechanism [30] and an exciton-polaron exchange process [30].

Similarly, there is substantial variation in the types of interactions assumed within the three-spin complex and the conditions under which they will be observed. TEP has been discussed in terms of weakly-interacting precursor pairs [22], strongly bound trion states [31], and even bipolaron-counterion complexes [26]. Each of these scenarios will produce a unique magnetic field dependence and differentiation is an important step towards purposeful tuning of spintronic devices. The conditions under which the TEP mechanism will appear are also debated: high magnetic-field features from magnetoconductance measurements indicate that the triplet process is important at room temperature [10], in contradiction with the sharp decrease in triplet lifetimes observed at high temperatures [32] and in earlier pEDMR experiments [33].

In this paper we develop a time-domain theory of an interacting spin-1 + spin-1/2 pair which can react in proportion to its overall doublet ($S = 1/2$) or quartet ($S = 3/2$) content, analogous to the theory of Ern and Merrifield [34]. The transition frequencies and resonance positions of an exciton-polaron complex are extracted from the canonical Hamiltonian, providing an analytic description of the transition between a weakly spin-interacting exciton-polaron complex and a strongly bound trion state. This result can be used to analyze pEDMR experiments on organic devices, allowing the intrapair spin-spin coupling to be extracted, as demonstrated in related work [35]. In this paper we concentrate on transitions following a single pulse; however, the formalism can be applied more generally to multipulse sequences, such as the Hahn echo [16,36]

$$\pi/2 - t - \pi - t - \pi/2 - \text{echo}, \tag{2}$$

where t is a variable free evolution period and $\pi/2$ and π represent the nominal spin nutation angles. This scheme measures the spin-spin relaxation time T_2 of a spin ensemble and can be simulated by applying a corresponding sequence of superoperators [14]. As such, this work provides a general foundation for the quantitative investigation of the triplet-exciton polaron quenching process with pEDMR.

II. GENERAL FEATURES

Long-lived triplet excitons can interact with trapped polarons to form complexes, which can recombine to release the trapped polaron and alter the free charge carrier density. Although a similar process is possible with singlet excitons, their density will be much lower [26] and we therefore ignore their contribution in this work. The spin-independent formation of exciton-polaron complexes is likely to be dominated by the reorganization energy associated with the shared lattice distortion [37] due to the weak spin interaction between the exciton and polaron.

Following its formation, an exciton-polaron complex may (i) dissociate back into its constituents or (ii) recombine if it is in the doublet (spin-1/2) manifold, which will release the trapped polaron into the valence or conduction band, increasing the charge carrier mobility [see Fig. 1(a)]. The exact states involved in the reaction are unclear. Weak spin coupling is observed experimentally [33], although strongly bound trion states could also form prior to recombination.

$$[\text{exciton} + \text{polaron}] \rightarrow \text{exciton} + \text{polaron}, \tag{3}$$

$$[\text{exciton} + \text{polaron}] \rightarrow [\text{trion}] \rightarrow S_0 + \text{polaron}^*, \tag{4}$$

where $[\cdots]$ represents a spatial correlation between the exciton and polaron which may sometimes by accompanied by spin-spin coupling and $*$ represents an excited state. Spin resonance causes a mixing of the doublet and quartet manifolds, causing a net change in the recombination rate and average charge carrier mobility (conductivity). As in the two spin polaron-pair case [12] the second order contributions due to the change in the electron and hole bath concentrations and mobilities are negligible; thus the expected changes in mobility are given by

$$\Delta\mu_e(t) = \tau_L(r_e(t) - r_{e,eq}), \tag{5}$$

$$\Delta\mu_h(t) = \tau_L(r_h(t) - r_{h,eq}), \tag{6}$$

where τ_L is the charge carrier lifetime and represents the characteristic time between exciton-polaron complex formation and either recombination or dissociation occurring (these lifetimes can be different for the electron and hole ensembles), μ are the electron and hole mobilities, and $R(t)$ and r_{eq} are the time-dependent and equilibrium recombination rates.

The increase in charge carrier mobility from recombination can yield either a current enhancement or quenching, depending on whether the majority or minority carriers are released. This counterintuitive behavior arises due to the interplay between Coulombic attraction and carrier transport [38]. In general, we expect the charge reaction to release the majority carrier and provide a current enhancement. In the unipolar regime, which we treat as electron rich, the change in current will be proportional to the number of released carriers, n_e,

$$\Delta I(t) = e\Delta\bar{\mu}_e(t)n_e, \tag{7}$$

where ΔI is the change in current, $\Delta\bar{\mu}$ is the time-dependent change in the average charge carrier mobility, and n_e is the free (electron) polaron density. For a general description of the spin dynamics, we need to include the interaction of the spin ensemble with the environment. This includes charge carrier generation, dissociation, recombination, and relaxation. These influences may be included through the stochastic Liouville equation [22]

$$\frac{\partial\rho}{\partial t} = \frac{i}{\hbar}[\rho, \mathscr{H}] + \mathscr{S}[\rho] + \mathscr{R}\{\rho - \rho_0\}, \tag{8}$$

where ρ is the density matrix and represents the occupation probability of each state, ρ_0 is the steady state density matrix, $\mathscr{H}$ is the coherent spin Hamiltonian and describes

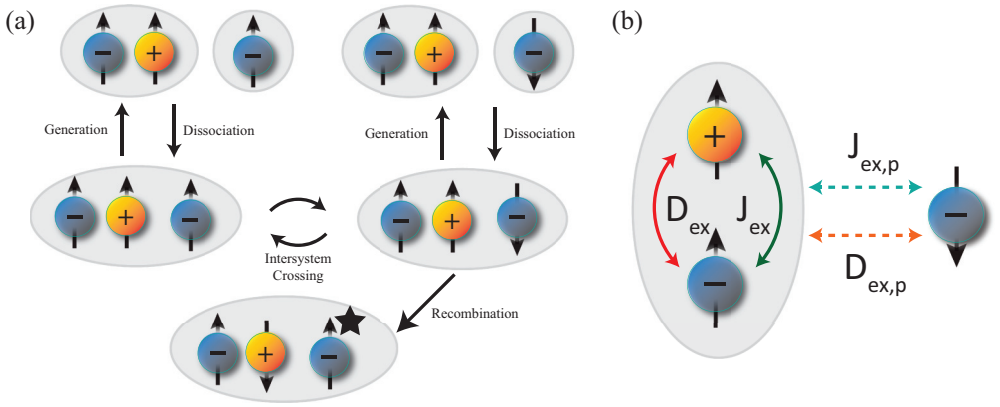

FIG. 1. (Color online) (a) General picture of the triplet exciton-polaron quenching mechanism. Exciton-polaron complexes are formed spin independently due to the reorganization energy associated with a shared nuclear distortion. A complex may spin independently dissociate back in a separate exciton and polaron or recombine, possibly due to weak exciton-polaron exchange. Intersystem crossing will mix the doublet and quartet states prior to recombination or dissociation. (b) A diagramatic representation of the Hamiltonian for an exciton-polaron complex with arbitrary coupling. The exciton will have internal exchange (J_{ex}) and dipolar (D_{ex}) coupling, and there may also be exchange ($J_{ex,p}$) and dipolar ($D_{ex,p}$) coupling between the exciton and the polaron.

the exciton-polaron spin complex, $\mathscr{S}$ is a stochastic operator and represents the generation and loss of charge carriers, and $\mathscr{R}$ is the Redfield relaxation matrix describing stochastic fluctuations between the spin ensemble and thermal bath, and which drives the density matrix into a diagonal thermal state [39,40].

A. Hamiltonian

The spin Hamiltonian describes the coupling within the exciton-polaron complex and its interactions with the surrounding nuclear environment. As it completely encapsulates the coherent spin dynamics it can be used to derive the resonance positions and transition frequencies which allow the mechanism and coupling strengths to be identified. Both the exciton and polaron couple to the nearby nuclei through the hyperfine interaction (A) and to the external magnetic field through Zeeman splitting. There is also dipolar coupling within the exciton (D_{ex}), and dipolar ($D_{ex,p}$) and exchange coupling ($J_{ex,p}$) between the exciton and polaron [see Fig. 1(b)]. The exciton has a large internal exchange ($J_{ex} \approx 0.7$ eV [41]) which separates the singlet and triplet levels. This is larger than all of the other energy scales in a typical experiment. This decouples the singlet levels and allows the exchange interaction to be excluded from the effective Hamiltonian,

$$\begin{aligned}\mathscr{H} = &\underbrace{\mu_B B \cdot g_{ex} \cdot S_{ex}}_{\text{exciton Zeeman}} + \underbrace{\mu_B B \cdot g_p \cdot S_p}_{\text{polaron Zeeman}} + \sum_i \underbrace{I_{ex,i} \cdot A_{ex,i} \cdot I_{ex,i}}_{\text{exciton hyperfine}} \\ &+ \sum_i \underbrace{I_{p,i} \cdot A_{p,i} \cdot I_{p,i}}_{\text{polaron hyperfine}} + \underbrace{S_{ex} \cdot D_{ex} \cdot S_{ex}}_{\text{exciton dipolar}} \\ &+ \underbrace{J_{ex,p} S_{ex} \cdot S_p}_{\text{exciton-polaron exchange}} + \underbrace{S_{ex} \cdot D_{ex,p} \cdot S_p}_{\text{exciton-polaron dipolar}}, \end{aligned} \tag{9}$$

where B is the external magnetic field, μ_B is the Bohr magneton, A is the hyperfine coupling tensor, g is the Landé g factor, I are the interacting nuclear spins, and S are the [exciton (ex) and polaron (p)] spin operators. An expanded version of this matrix is given in Appendix A. The commonly used high field approximations are made, which include an isotropic g factor, isotropic hyperfine interaction, and only retaining the secular terms of the dipolar coupling [40].

Starting from the triplet-doublet (product) basis we can rotate the Hamiltonian to the energy eigenbasis using the unitary transform [42]

$$\mathscr{H}_{\text{energy}} = U^{\dagger} \mathscr{H} U, \tag{10}$$

where

$$U = \begin{bmatrix} 1 & 0 & 0 & 0 & 0 & 0 \\ 0 & \cos\theta & 0 & -\sin\theta & 0 & 0 \\ 0 & 0 & \cos\phi & 0 & \sin\phi & 0 \\ 0 & \sin\theta & 0 & \cos\theta & 0 & 0 \\ 0 & 0 & -\sin\phi & 0 & \cos\phi & 0 \\ 0 & 0 & 0 & 0 & 0 & 1 \end{bmatrix}, \tag{11}$$

with

$$\cot 2\theta = \frac{D_{ex} - \frac{D_{ex,p}}{3} + \frac{J_{ex,p}}{2} - \omega_p + \omega_{ex}}{\frac{\sqrt{2}D_{ex,p}}{3} + \sqrt{2}J_{ex,p}} \tag{12}$$

and

$$\cot 2\phi = \frac{D_{ex} - \frac{D_{ex,p}}{3} + \frac{J_{ex,p}}{2} + \omega_p - \omega_{ex}}{\frac{\sqrt{2}D_{ex,p}}{3} + \sqrt{2}J_{ex,p}}. \tag{13}$$

These mixing angles can be easily computed by noting that the 6×6 Hamiltonian can be two decomposed into two 1×1 subspaces, which are already diagonal, and two 2×2 sub-spaces which can be diagonalized by applying the standard rotation matrices [43]. This unitary transform preserves the physics of the Hamiltonian, while simplifying analytic and numerical calculations. For instance, the transition frequencies simply correspond to the off-diagonal matrix elements. Importantly, the angles θ and ϕ represent the degree of coupling between the exciton and polaron. Setting $\theta, \phi = 0$ corresponds to two independent particles and $\theta, \phi = \cos^{-1}\sqrt{\frac{2}{3}}$ (the maximum rotation angle possible) corresponds to the formation of a spin-$\frac{3}{2}$ trion. Due to the convenient measure

of spin-spin coupling that θ and ϕ provide we will refer to them throughout the text as the *spin mixing angles*.

The three natural basis sets for describing an exciton-polaron complex are the triplet-doublet (product) basis, the quartet-doublet basis, and the energy eigenbasis. The transformation between the triplet-doublet and quartet-doublet bases is given by the Clebsch-Gordan coefficients:

$$|T_+\uparrow\rangle = |Q_{3/2}\rangle, \tag{14}$$

$$|T_+\downarrow\rangle = \sqrt{\frac{1}{3}}|Q_{1/2}\rangle + \sqrt{\frac{2}{3}}|D_{1/2}\rangle, \tag{15}$$

$$|T_0\uparrow\rangle = \sqrt{\frac{2}{3}}|Q_{1/2}\rangle - \sqrt{\frac{1}{3}}|D_{1/2}\rangle, \tag{16}$$

$$|T_0\downarrow\rangle = \sqrt{\frac{1}{3}}|Q_{-1/2}\rangle + \sqrt{\frac{2}{3}}|D_{-1/2}\rangle, \tag{17}$$

$$|T_-\uparrow\rangle = -\sqrt{\frac{2}{3}}|Q_{-1/2}\rangle + \sqrt{\frac{1}{3}}|D_{-1/2}\rangle, \tag{18}$$

$$|T_-\downarrow\rangle = |Q_{-3/2}\rangle, \tag{19}$$

where D and Q represent the doublet and quartet states with their spin projection given by the subscripts. It is important to note that the term "doublet" refers to a state with $S = 1/2$, which may either be a single spin-1/2 particle or the $|S,m_s\rangle = |\frac{1}{2},\pm\frac{1}{2}\rangle$ trion states. The density matrix

$$\rho = \sum_i w_i \,|\rho_i\rangle\,\langle\rho_i| \tag{20}$$

(where w_i is the spin level occupation) can likewise be transformed from the triplet doublet to the energy eigenbasis by

$$\rho_{\text{energy}} = U^\dagger \rho U. \tag{21}$$

In the triplet-doublet basis the kets are given by

$$|\rho\rangle = \begin{bmatrix} |T_+\uparrow\rangle \\ \cos\theta\,|T_0\uparrow\rangle + \sin\theta\,|T_+\downarrow\rangle \\ \cos\phi\,|T_-\uparrow\rangle - \cos\phi\,|T_0\downarrow\rangle \\ \cos\theta\,|T_+\downarrow\rangle - \sin\theta\,|T_0\uparrow\rangle \\ \cos\phi\,|T_0\downarrow\rangle + \sin\phi\,|T_-\uparrow\rangle \\ |T_-\downarrow\rangle \end{bmatrix}. \tag{22}$$

It is conceptually and computationally expedient to split the Hamiltonian into a large static component (H_0) comprising spin-spin coupling terms and the static Zeeman splitting, and a small, time-dependent driving term (H_1) which corresponds to the time-dependent Zeeman splitting:

$$\mathscr{H} = \mathscr{H}_0 + \mathscr{H}_1, \tag{23}$$

$$\mathscr{H}_1 = 2B_1(e^{-i\omega t} + e^{i\omega t})\left(S_{ex}^x + S_p^x\right), \tag{24}$$

where S is the spin operator for the exciton and polaron and ω is the frequency of the applied radiation. At high field the counterpropagating component will produce no first-order effects, so we move to the rotating frame and perform the rotating wave approximation. This is done for all the following calculations and we denote the new Hamiltonian by $\mathscr{H}^*$ to indicate that we are treating dressed states:

$$\mathscr{H}_{\text{rot}} = U_{\text{rot}}^\dagger \mathscr{H} U_{\text{rot}} - U_{\text{rot}}^\dagger \frac{\partial \mathscr{H}}{\partial t} U_{\text{rot}}, \tag{25}$$

$$U_{\text{rot}}(t) = e^{-iB_0(S_{ex}^z + S_p^z)t}. \tag{26}$$

The rotating frame will shift the energy of the static Hamiltonian H_0, so the new static rotating component H_0^* is

$$\mathscr{H}_0^* = \mathscr{H}_0 - B_0\left(S_{ex}^z + S_p^z\right) \tag{27}$$

and the resonant driving will become time independent, so the new Hamiltonian is

$$\mathscr{H}^* = \begin{bmatrix} E_1^* & B_{12} & 0 & B_{14} & 0 & 0 \\ B_{21} & E_2^* & B_{23} & 0 & B_{25} & 0 \\ 0 & B_{32} & E_3^* & B_{34} & 0 & B_{36} \\ B_{41} & 0 & B_{43} & E_4^* & B_{45} & 0 \\ 0 & B_{52} & 0 & B_{54} & E_5^* & B_{56} \\ 0 & 0 & B_{63} & 0 & B_{65} & E_6^* \end{bmatrix}, \tag{28}$$

where the energies of H_0 are given by coefficients E_i and coherent mixing terms due to H_1 are given by the coefficients B_{ij}. These can be found in Appendix A. The dressed rotating basis states will have the same form as the bare energy eigenbasis states, and for most situations they may be treated equivalently [14].

B. Limiting behavior of the Hamiltonian

While numerical calculations provide a general method for calculating the exciton-polaron dynamics from the spin Hamiltonian, this approach limits the physical insight which we can obtain. To understand the general properties of the system we now look at a number of limiting cases.

1. Weak coupling: $\theta,\phi \to 0$

When the exciton-polaron coupling is extremely weak ($\theta,\phi \to 0$) the spins will be driven independently, and the eigenbasis is trivially given by the product states. The Hamiltonian for this scenario is

$$\mathscr{H}^* = \frac{\hbar}{2}\begin{bmatrix} E_{T_+\uparrow}^* & \sqrt{2}B_1 & 0 & B_1 & 0 & 0 \\ \sqrt{2}B_1 & E_{T_0\uparrow}^* & \sqrt{2}B_1 & 0 & B_1 & 0 \\ 0 & \sqrt{2}B_1 & E_{T_-\uparrow}^* & 0 & 0 & B_1 \\ B_1 & 0 & 0 & E_{T_+\downarrow}^* & \sqrt{2}B_1 & 0 \\ 0 & B_1 & 0 & \sqrt{2}B_1 & E_{T_0\downarrow}^* & \sqrt{2}B_1 \\ 0 & 0 & B_1 & 0 & \sqrt{2}B_1 & E_{T_-\downarrow}^* \end{bmatrix} \tag{29}$$

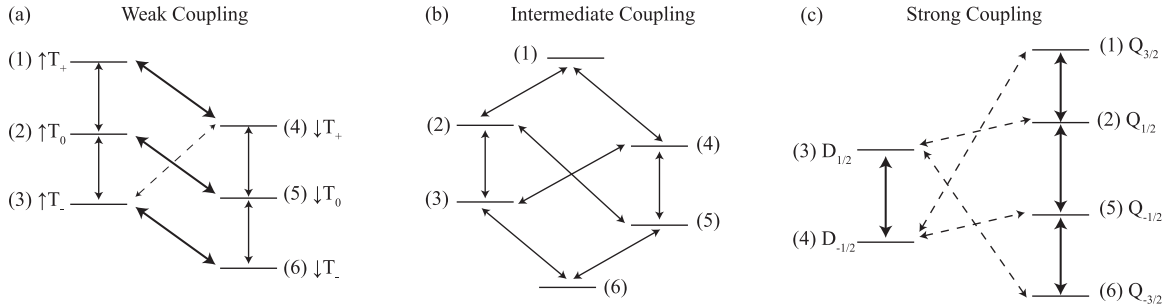

FIG. 2. Behavior of an exciton-polaron complex depends strongly on the strength of the exciton-polaron coupling. Solid lines represent strongly driven transitions and dashed lines represent transitions which become forbidden in the weak or strong coupling limits. (a) In the weak coupling regime the basis states are close to the product states and the transitions are the $|\uparrow\rangle \leftrightarrow |\downarrow\rangle$ polaron transition, with a Rabi frequency of γB_1, and the $|T_+\rangle \leftrightarrow |T_0\rangle$, $|T_0\rangle \leftrightarrow |T_-\rangle$ exciton transitions with a Rabi frequency of $\sqrt{2}\gamma B_1$. The $|\downarrow T_+\rangle \leftrightarrow |\uparrow T_-\rangle$ transition becomes weakly allowed in the presence of nonzero coupling. (b) In the intermediate coupling regime the basis states are neither the product nor quartet-doublet states and there are up to eight visible transitions with Rabi frequencies between zero and $\sqrt{3}\gamma B_1$. (c) In the strongly coupled regime quartets and doublets are formed. Strong driving occurs within the doublet and quartet manifolds and driving between the manifolds becomes arbitrarily slow, leading to a vanishing signal. The Rabi frequencies of these transitions are $\sqrt{3}\gamma B_1$ and $2\gamma B_1$.

and the basis kets are

$$|\rho\rangle = \begin{bmatrix} T_+\uparrow \\ T_0\uparrow \\ T_-\uparrow \\ T_+\downarrow \\ T_0\downarrow \\ T_-\downarrow \end{bmatrix}. \tag{30}$$

The polaron resonances occur at a frequency of $\omega + \omega_p$ with a Rabi (nutation) frequency of γB_1 and the exciton will resonate at frequencies of $\omega + \omega_{ex} \pm D_{ex}$ with a nutation frequency of $\sqrt{2}\gamma B_1$, where ω_p and ω_{ex} are the Zeeman components of the polaron and exciton energies. This is shown graphically in Fig. 2(a). There are three degenerate polaron transitions and a pair of two degenerate exciton transitions (with $|\uparrow T_+\rangle \leftrightarrow |\uparrow T_0\rangle$ and $|\downarrow T_+\rangle \leftrightarrow |\downarrow T_0\rangle$ forming one pair and $|\uparrow T_0\rangle \leftrightarrow |\uparrow T_-\rangle$ and $|\downarrow T_0\rangle \leftrightarrow |\downarrow T_-\rangle$ forming the other). These are shown by the solid lines. The single dashed line represents a $\Delta m_s = 1$ transition between the $|\uparrow T_-\rangle$ and $|\downarrow T_+\rangle$ states which becomes weakly allowed in the presence of nonzero exciton-polaron coupling. Eventually the spin-spin coupling becomes large compared to the hyperfine interaction and the transitions can no longer be described as excitonic or polaronic transitions, as depicted in Fig. 2(b).

2. *Strong coupling:* $\theta,\phi \rightarrow \cos^{-1}(\sqrt{\frac{2}{3}})$

When the exciton-polaron coupling is extremely strong $[\theta,\phi \rightarrow \cos^{-1}(\sqrt{\frac{2}{3}})]$ a trion state will be formed in the quartet-doublet basis. The exciton and polaron can no longer be considered separate entities and they will always nutate together. The Hamiltonian is given by

$$\mathscr{H}^* = \frac{\hbar}{2}\begin{bmatrix} E^*_{Q=\frac{3}{2}} & \sqrt{3}B_1 & 0 & 0 & 0 & 0 \\ \sqrt{3}B_1 & E^*_{Q=\frac{1}{2}} & 0 & 0 & 2\gamma B_1 & 0 \\ 0 & 0 & E^*_{D=\frac{1}{2}} & \gamma B_1 & 0 & 0 \\ 0 & 0 & \gamma B_1 & E^*_{D=-\frac{1}{2}} & 0 & 0 \\ 0 & 2\gamma B_1 & 0 & 0 & E^*_{Q=-\frac{1}{2}} & \sqrt{3}B_1 \\ 0 & 0 & 0 & 0 & \sqrt{3}B_1 & E^*_{Q=-\frac{3}{2}} \end{bmatrix}, \tag{31}$$

with the corresponding eigenstates

$$|\rho\rangle = \begin{bmatrix} Q_{\frac{3}{2}} \\ Q_{\frac{1}{2}} \\ D_{\frac{1}{2}} \\ D_{-\frac{1}{2}} \\ Q_{-\frac{1}{2}} \\ Q_{-\frac{3}{2}} \end{bmatrix}. \tag{32}$$

The mixing will be between the $m_s = \pm 3/2$ and $m_s = \pm 1/2$ quartet manifolds with nutation frequency of $\sqrt{3}\gamma B_1$, and mixing within the $m_s = \pm 1/2$ doublet and quartet manifolds with Rabi frequencies of γB_1 and $2\gamma B_1$, as shown in Fig. 2(c). The four solid lines represent the strongly allowed transitions of the trion state and the dashed lines represent quartet-doublet transitions which vanish in the strong coupling regime. Counterintuitively the $m_s = \pm 3/2$ quartet states actually couple to the $m_s = \mp 1/2$ doublet states, which is nominally a $\Delta m_s = 2$ transition. Analogous to the exciton half-field transition, it

becomes weakly allowed due to off-diagonal mixing in the quartet-doublet basis. Because the strongly allowed transitions induce no overall change in the doublet or quartet content of the complex, the trion states will be electrically undetectable.

In this paper we analyze the transition between the uncoupled and trionic regimes.

C. Complex relaxation and recombination

The recombination and dissociation rates of each eigenstate will be the weighted average of its quartet and doublet content. In analogy with the polaron pair [12] case we can form new rates for the admixture states,

$$r_i = r_D |\langle i|D\rangle|^2 + r_Q |\langle i|Q\rangle|^2, \tag{33}$$

$$d_i = d_D |\langle i|D\rangle|^2 + d_Q |\langle i|Q\rangle|^2, \tag{34}$$

where $|i\rangle$ represent the general eigenkets, D and Q represent the doublet and quartet manifolds, and r and d are the recombination and dissociation rates for the doublet and quartet states. The spin loss rate (γ) is the sum of the dissociation and recombination rates:

$$\gamma_i = r_i + d_i. \tag{35}$$

A spin-dependent depopulation of the doublet state has been observed in other systems and is consistent with simple energetic arguments and spin-selection rules [44]. In the weak coupling limit ($\theta,\phi \to 0$) the $T_-\uparrow, T_+\downarrow$ states have $\frac{2}{3}$ doublet content, and the T_0 states each have $\frac{1}{3}$ doublet content. The recombination rates r_i from Eq. (33) are then

$$r = \frac{1}{3}\begin{bmatrix} 3r_Q \\ r_D + 2r_Q \\ 2r_D + r_Q \\ 2r_D + r_Q \\ r_D + 2r_Q \\ 3r_Q \end{bmatrix}. \tag{36}$$

In the opposite, strong coupling limit ($\theta,\phi \to \cos^{-1}\sqrt{\frac{2}{3}}$) the states become pure quartet and doublet states, with the corresponding recombination rates

$$r = \begin{bmatrix} r_Q \\ r_Q \\ r_D \\ r_D \\ r_Q \\ r_Q \end{bmatrix}. \tag{37}$$

Between these two limits there will be a monotonic change in the recombination rates as the product basis morphs into the quartet-doublet basis.

D. Complex formation and polarization

We cannot discuss the transitions of an exciton-polaron complex without discussing their formation and steady state polarization: the presence of an electrically detectable signal intrinsically requires a net transfer of the spin population.

Exciton-polaron complexes are believed to form spin independently. A spin-dependent formation has been proposed in the context of polaron pairs, and a similar effect for exciton polarons will change the intensity of the transitions, but leave the qualitative conclusions of this study unaffected. Regardless, the generation rate of each state needs to be weighted by a Boltzmann factor to account for the thermal distribution:

$$G_i = G\frac{\exp\left(-\frac{E_i}{kT}\right)}{\sum_i \exp\left(-\frac{E_i}{kT}\right)}, \tag{38}$$

where G is the total generation rate, G_i is the generation rate for each eigenstate, k is the Boltzmann constant, and T is the sample temperature. These generation rates provide the diagonal entries for the creation component of the stochastic operator $\mathscr{S}$. At high temperatures polarization effects can be ignored and a uniform generation rate can be used. The steady state occupation of each state corresponds to when the pair generation and loss rates are equal:

$$\rho_{ii} = \frac{G_i}{r_i + d_i}. \tag{39}$$

When doublet states are lost much faster than quartet states there will be a strong polarization of pure quartet states:

$$\rho_0 = \tfrac{1}{2}(|T_+\uparrow\rangle\langle T_+\uparrow| + |T_-\downarrow\rangle\langle T_-\downarrow|). \tag{40}$$

In organic devices the polarization effects arise primarily from the different rates of charge carrier loss [12]. In contrast, porphyrin systems may generate a polarization within the triplet-doublet pairs from the intersystem crossing of light-induced singlet-doublet states [45–47].

E. Transient readout

The real-time detection of sample conductivity changes during resonant excitation is technologically challenging [48]. Consequently, experiments are usually performed using a pump-probe approach, which involves monitoring the (slow) response of the system following (rapid) magnetic resonant excitation [12].

In the triplet-exciton polaron quenching mechanism recombination will trap or detrap the polaron and change the average charge carrier mobility. This manifests macroscopically as a change in the sample conductivity. We can therefore relate the recombination rate (proportional to the overall doublet content of the spin ensemble in our model) to an experimental change in conductivity. Larmor beating will dephase the exciton and polaron on a time scale much faster than the transient readout, and we can therefore treat the spin ensemble incoherently using rate equations [24]

$$R(\tau) = \sum_i \delta\rho_{ii}(\tau) r_i, \tag{41}$$

where $\delta\rho_{ii}$ is the change in occupation probability and r_i the recombination rate of each state. The overall change in current induced by each transition will depend on the precise choice of integration window and dissociation, recombination, and intersystem crossing rates. In this work, we are concerned with the resonance positions and transition frequencies, which are unaffected by these incoherent rates. Nonetheless, we sketch how quantitative predictions may be made by discussing the

minimalist scenario in which intersystem crossing and recombination are slow compared to dissociation. This produces an observable which is proportional to the doublet content of the occupied states. We also assume that all recombination events are recorded,

$$O = \sum_i \int_0^T r_i \exp(-(r_i + d_i)t)dt \approx \sum_i \frac{r_i}{d_i} \approx \sum_i |\langle D|\phi_i\rangle|^2, \quad (42)$$

where ϕ_i is the ith eigenvector, D is the doublet manifold, and O is the observed change in sample conductivity. A scaling factor is required to relate the microscopic change in charge carrier mobility to the real change in sample conductivity.

III. TRANSITION ANALYSIS

In the standard implementation of a pEDMR experiment the transition frequencies are mapped as a function of energy by sweeping the magnetic field with a constant excitation frequency and measuring the change in conduction as a function of the microwave pulse length. This may result in a number of different resonances each with a particular transition frequency. These serve as a "Rabi fingerprint," which can be used to identify and quantify the types of coupling present. We now calculate these "fingerprints" directly from the spin Hamiltonian.

A. Resonance position

The photon energy required to resonantly drive a transition is equal to the energy difference between the two eigenstates of interest. The energies of the Hamiltonian described by Eqs. (A2)–(A7) are used to calculate the resonance positions given in Table III.

In the weak coupling limit there are three polaron transitions, which occur at the Larmor precession frequency, and four exciton transitions, which are split by the intraexciton dipolar coupling D_{ex}. The multiplicity of each transition is due to possible states of its partner, so the exciton has identical transitions whether the polaron is in the $|\uparrow\rangle$ or $|\downarrow\rangle$ state. In the strong-coupling limit the $m_s = 1/2$ transitions ($Q_{\frac{1}{2}} \leftrightarrow Q_{-\frac{1}{2}}$, $D_{\frac{1}{2}} \leftrightarrow D_{-\frac{1}{2}}$) will occur at the Larmor precession frequency and the other quartet resonances ($Q_{\pm\frac{3}{2}} \leftrightarrow Q_{\pm\frac{1}{2}}$) will have significantly higher or lower Larmor frequencies due to the substantial zero-field splitting.

B. Transition frequencies

The frequency of the Rabi oscillations are indicative of the types of states and coupling that are present, and are calculated by solving the 2×2 eigenvalue problem of the relevant subspace [25]

$$\mathscr{H}_{2\times 2} = \begin{pmatrix} E_i & B_{ij} \\ B_{ji} & E_j \end{pmatrix}. \quad (43)$$

The frequencies of the Rabi oscillations have the form

$$\Omega_{ij} = \sqrt{\alpha_{ij}^2(\gamma B_1)^2 + (\omega - \omega_{ij})^2}, \quad (44)$$

TABLE I. Transition frequencies of an exciton-polaron complex as a function of the spin mixing angles.

Transition	Frequency (γB_1)
(1)-(2)	$\sqrt{2}\cos\theta + \sin\theta$
(1)-(4)	$\cos\theta - \sqrt{2}\sin\theta$
(2)-(3)	$\sqrt{2}\cos\theta\cos\phi - \sin\phi(\cos\theta + \sqrt{2}\sin\theta)$
(2)-(5)	$\cos\phi(\cos\theta + \sqrt{2}\sin\theta) + \sqrt{2}\cos\theta\sin\phi$
(3)-(4)	$\sin\theta(\sin\phi - \sqrt{2}\cos\phi) - \sqrt{2}\cos\theta\sin\phi$
(3)-(6)	$\cos\phi - \sqrt{2}\sin\phi$
(4)-(5)	$-\cos\phi(\sin\theta - \sqrt{2}\cos\theta) - \sqrt{2}\sin\theta\sin\phi$
(5)-(6)	$\sin\phi + \sqrt{2}\cos\phi$

where α_{ij} is the frequency coefficient which may be read from the off-diagonal matrix entries which are given by $\mathscr{H}^*$ in Eq. (31), ω is the applied photon frequency, and ω_{ij} is the resonant (i, j) transition frequency. When a resonant excitation ($\omega = \omega_{ij}$) is applied the nutation frequency reduces to

$$\Omega_{ij} = \alpha_{ij}\gamma B_1. \quad (45)$$

The values for all nonzero α_{ij} coefficients are given in Table I and are shown graphically in Fig. 3 as a function of the mixing angle θ (with $\theta = \phi$). It can be seen that the nutation frequencies change distinctively as a function of mixing angle, and this can be used to differentiate triplet-exciton polaron quenching from other mechanisms such as the triplet-triplet annihilation, as well as identifying the relevant coupling regime.

C. Regimes

We are able to identify several driving regimes depending on the relative energy scales present. Figure 3 shows the

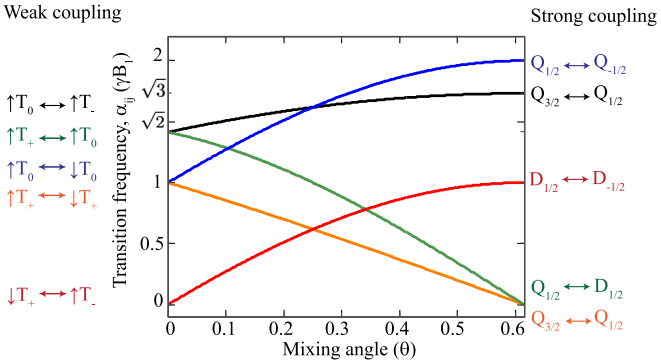

FIG. 3. (Color online) Transition frequencies of an exciton-polaron complex as a function of the mixing angle. In the uncoupled regime ($\theta = 0$) the polaron will nutate at a frequency of γB_1 and the exciton will nutate at a frequency of $\sqrt{2}\gamma B_1$. Weak coupling splits the exciton and polaron resonances and permits the $\downarrow T_+ \leftrightarrow \uparrow T_-$ transition to be weakly driven. In the strong coupling limit pure quartet and doublet states are formed. Quartet mixing will occur at frequencies of $2\gamma B_1$ ($Q_{1/2} \leftrightarrow Q_{-1/2}$) and $\sqrt{3}\gamma B_1$ ($Q_{\pm 3/2} \leftrightarrow Q_{\pm 1/2}$). Driving can also occur within the doublet manifold at a frequency of γB_1. Driving between the doublet and quartet states becomes arbitrarily slow in the strong coupling limit. Transition frequencies are calculated by using Eq. (45).

transition frequencies as a function of mixing angle. Additional regimes are possible when the exchange and dipolar coupling are able to cancel out on either the diagonal or off-diagonal elements of the Hamiltonian.

Uncoupled regime. This is the simplest case, in which there is no interaction between the exciton and polaron ($J_{ex,p}, D_{ex,p} = 0$). The polaron will nutate at γB_1 and the exciton will be split into two lines, each with a transition frequency of $\sqrt{2}\gamma B_1$. When there is no intraexciton dipolar coupling ($D_{ex} = 0$), the exciton levels become harmonically spaced and a multitransition analysis is required, which we do not treat in this paper.

Effectively uncoupled regime. Similar behavior occurs in the effectively uncoupled regime, which occurs when $|D_{ex,p} + 3J_{ex,p}| << D_{ex}$. The off-diagonal mixing vanishes and the physics will be identical to the weakly coupled regime except that the transitions have a greater splitting.

Weakly coupled regime. The generic weakly coupled regime corresponds to when there is a small exciton-polaron coupling ($|D_{ex,p}|, |J_{ex,p}| << D_{ex}$) as compared with the hyperfine and intraexciton dipolar (D_{ex}) coupling. The exciton and polaron resonances become weakly correlated—the $|T_+\uparrow\rangle \leftrightarrow |T_+\downarrow\rangle$ and $|T_0\uparrow\rangle \leftrightarrow |T_0\downarrow\rangle$ transitions will have slightly different transition frequencies, for instance, and the $|T_+\downarrow\rangle \leftrightarrow |T_-\uparrow\rangle$ transition becomes weakly allowed and will provide a low frequency background.

Isoenergetic regime. An interesting case occurs when $D_{ex,p} = \frac{3}{2}J_{ex,p}$ and $J_{ex,p} << D_{ex}$. The energy levels will be unshifted to first order, but there will be a small shift in the transition frequencies and the effective recombination rates.

Trionic regime. The trionic regime will occur when there is strong exchange or dipolar coupling between the exciton and polaron states. In either case, the exciton and polaron become strongly entangled and form either quartet or doublet states. Driving between the quartet and doublet states ($|Q_{\pm\frac{3}{2}}\rangle \leftrightarrow |D_{\mp\frac{1}{2}}\rangle$, $|Q_{\pm\frac{1}{2}}\rangle \leftrightarrow |D_{\pm\frac{1}{2}}\rangle$) will have a vanishingly small probability. Driving will also occur between the doublet states ($|D_{\frac{1}{2}}\rangle \leftrightarrow |D_{-\frac{1}{2}}\rangle$) at a frequency of γB_1 and between the quartet states ($|Q_{\pm\frac{3}{2}}\rangle \leftrightarrow |Q_{\pm\frac{1}{2}}\rangle$, $|Q_{\frac{1}{2}}\rangle \leftrightarrow |Q_{-\frac{1}{2}}\rangle$) at frequencies of $\sqrt{3}\gamma B_1$ and $2\gamma B_1$, respectively. As these transitions leave the overall quartet-doublet content unchanged, they will not produce an observable signal in the absence of spin-orbit coupling or some other additional spin-reaction pathway.

Intermediate coupling regime. Between these two extremes lies the intermediate coupling regime which involves neither pure triplet-doublet, nor quartet-doublet basis states. There will be eight possible transitions with frequencies between zero and three γB_1. Due to the large parameter space this regime encompasses, a numerical approach is usually required.

We have so far dealt with an exciton interacting with a polaron, which corresponds to positive exchange and dipolar coupling using our definition. A bipolaron interacting with a counterion can be treated by including negative exchange and dipolar coupling, a scenario advocated by Shinar [26].

Once again we can precisely extract the spin-spin coupling from the Rabi fingerprint. Weak coupling produces individually excitable bipolaron and counterion states with characteristic Rabi frequencies of γB_1 and $\sqrt{2}\gamma B_1$. As the coupling strength is increased the bipolaron will be torn apart,

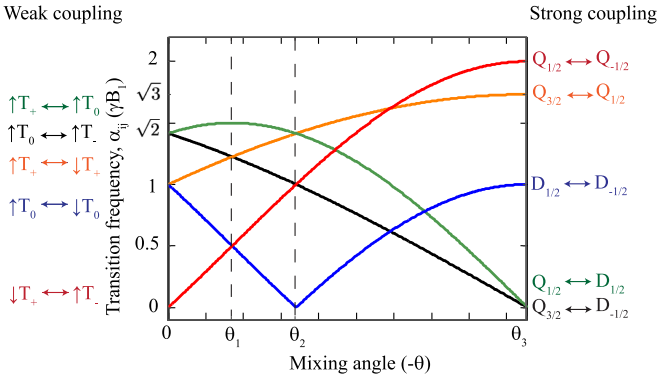

FIG. 4. (Color online) Transition frequencies of a bipolaron counterion complex, which is treated by introducing a negative mixing angle. At an angle of $\theta_1 = \frac{\cos^{-1}\sqrt{\frac{2}{3}} - \cos^{-1}\sqrt{\frac{1}{3}}}{2}$ the bipolaron is broken apart by the strong Coulombic attraction from the counterion. If the coupling is increased further an exciton-polaron complex is formed for a mixing angle of $\theta_2 = \cos^{-1}\sqrt{\frac{2}{3}} - \cos^{-1}\sqrt{\frac{1}{3}}$. From mixing angles of θ_2 to $\theta_3 = \cos^{-1}\sqrt{\frac{1}{3}}$ the transition frequencies of the exciton-polaron complex evolve in an identical manner to the positive mixing angle regime. Transition frequencies are calculated from Eq. (45).

which occurs at a mixing angle of

$$\theta_1 = \frac{\cos^{-1}\sqrt{\frac{2}{3}} - \cos^{-1}\sqrt{\frac{1}{3}}}{2} \tag{46}$$

and can be seen as a frequency degeneracy in Fig. 4. If the spin-spin coupling is increased, then an exciton-polaron complex will be formed at a spin mixing angle of

$$\theta_2 = \cos^{-1}\sqrt{\frac{2}{3}} - \cos^{-1}\sqrt{\frac{1}{3}}. \tag{47}$$

This produces Rabi frequencies of γB_1 and $\sqrt{2}\gamma B_1$, as expected. After this point the states may form a trion, proceeding in a similar manner to above with a maximum mixing angle of

$$\theta_3 = \cos^{-1}\sqrt{\frac{1}{3}} \tag{48}$$

indicating the complete formation of a spin-3/2 particle. The transition between each of these regimes is shown in Fig. 4.

IV. HALF-FIELD

It is possible to directly excite a "$\Delta m_s = 2$" spin-flip transition between the T_- and T_+ states of an exciton at the half-field resonance:

$$\frac{\mathcal{H}_1}{\hbar} = 2\gamma B_1\left[S_{ex}^x + S_p^x\right](e^{2i\omega t} + e^{-2i\omega t}). \tag{49}$$

This transition is nominally forbidden, but becomes weakly allowed due to off-diagonal zero-field splitting which suppresses spin as a good quantum number and creates admixtures of the T_+ and T_- states.

To perform quantitative analysis of the half-field transitions it is necessary to move to the doubly rotating frame and expand

the time-averaged Hamiltonian to second order [14]

$$\bar{\mathscr{H}} = \frac{1}{\tau_c}\int_0^{\tau_c} \mathscr{H}(t)dt - \frac{i}{2\tau_c}\int_0^{\tau_c}\int_0^{t_2} [\mathscr{H}(t_2),\mathscr{H}(t_1)]dt_1 dt_2, \tag{50}$$

where $\bar{\mathscr{H}}$ is the average Hamiltonian, τ_c is the period of the perturbation, and $\mathscr{H}$ is the original Hamiltonian. This produces a term proportional to

$$\frac{B_1 D \sin 2\theta}{B_0}(S_+S_+ + S_-S_-), \tag{51}$$

which is responsible for the $\Delta m_s = 2$ transition. To obtain the correct transition probability, it is necessary to integrate over all the possible orientations with the appropriate weighting. The ensemble half-field Rabi frequency will scale with the driving field and dipolar strength in the perturbative regime.

V. MICROSCOPIC BASIS FOR RECOMBINATION

So far we have discussed the spin-dependent recombination of exciton-polaron complexes. An obvious argument to account for the different rates is spin conservation: the ground state is $S = 1/2$, so we should expect the doublet states to decay faster than the quartet states; however, this ignores the fact that both are orthogonal to the ground state:

$$\left\langle Q|0,\tfrac{1}{2}\right\rangle = 0, \tag{52}$$

$$\left\langle D|0,\tfrac{1}{2}\right\rangle = 0. \tag{53}$$

We propose a possible mechanism in which spin conservation holds, yet allows spin angular momentum to be transferred between the exciton and polaron: a Dexter exchange-based pathway [49] reliant on a small asymmetry in the exciton-polaron exchange. In the canonical Hamiltonian it is tacitly assumed that the exchange between the lone polaron and each of the constituent polarons are equal. Due to the opposite polarity of the exciton polarons, one would expect there to be a small asymmetry in the two coupling strengths [25]:

$$J_{ex,p,\mathrm{tot}} = J_{ex,p} + \Delta J_{ex,p}, \tag{54}$$

where $J_{ex,p,\mathrm{tot}}$ is the total exchange coupling between the exciton and polaron, $J_{ex,p}$ is the sum of the two microscopic exchange interactions, and $\Delta J_{ex,p}$ is a small asymmetry between the electron-polaron and hole-polaron exchange couplings (see Table II):

$$\Delta J_{ex,p} = S_{e,ex}\cdot S_{e,p} - S_{h,ex}\cdot S_{e,p}. \tag{55}$$

The asymmetric exciton-polaron exchange interaction ($\Delta J_{ex,p}$) is isotropic and will be small in comparison with the exciton exchange (J_{ex}). The new eigenstates may be efficiently calculated analytically or numerically, but are generally cumbersome to deal with. A fruitful path is to examine the role of exciton-polaron exchange through first order perturbation theory [43]:

$$\Delta_n = \langle n^0|\Delta J_{ex,p}|n^0\rangle, \tag{56}$$

$$|n\rangle = |n^{(0)}\rangle + \Sigma_{k\neq n}|k^{(0)}\rangle\frac{V_{kn}}{E_n^{(0)} - E_k^{(0)}}, \tag{57}$$

TABLE II. Unnormalized eigenkets of a weakly coupled exciton-polaron complex when there is a small difference in the exchange coupling. The resultant mixing between singlet and triplet manifolds allows recombination of the doublet states to the singlet ground state.

No exchange	Exchange
$\uparrow T_+$	$\uparrow T_+$
$\uparrow S$	$\uparrow S + \frac{\Delta J_{ex,p}}{J_{ex}+\frac{D_{ex}}{6}} T_0 - \frac{\sqrt{2}\Delta J_{ex,p}}{J_{ex}-\frac{D_{ex}}{6}}\downarrow T_+$
$\uparrow T_0$	$\uparrow T_0 - \frac{\Delta J_{ex,p}}{J_{ex}+\frac{D_{ex}}{6}} S$
$\uparrow T_-$	$\uparrow T_- - \frac{\sqrt{2}\Delta J_{ex,p}}{J_{ex}-\frac{D_{ex}}{6}}\downarrow S$
$\downarrow T_+$	$\downarrow T_+ + \frac{\sqrt{2}\Delta J_{ex,p}}{J_{ex}-\frac{D_{ex}}{6}}\uparrow T_-$
$\downarrow S$	$\uparrow S + \frac{\Delta J_{ex,p}}{2(J_{ex}-\frac{D_{ex}}{3})}\uparrow T_0 + \frac{\Delta J_{ex,p}}{2(J_{ex}-\frac{D_{ex}}{6})}\downarrow T_+$
$\downarrow T_0$	$\downarrow T_0 + \frac{\Delta J_{ex,p}}{J_{ex}+\frac{D_{ex}}{3}}\downarrow S$
$\downarrow T_-$	$\downarrow T_-$

where Δ_n is the energy shift, $|n\rangle$ are the new eigenstates in terms of the uncoupled states, $|n^{(0)}\rangle$ and $|k^0\rangle$ are the unperturbed eigenstates, $E^{(0)}$ are the unperturbed energies of the eigenstates, and V_{kn} are the off-diagonal matrix elements of the perturbation. The resulting eigenkets are given in Eq. (C1).

In this mechanism the exciton-polaron recombination occurs due to the doublet states becoming mixed with the singlet exciton. This in turn depends on the relative exchange strengths

$$\langle S|D\rangle \approx \frac{\Delta J_{ex,p}}{J_{ex}}, \tag{58}$$

where S is the singlet manifold and D is the doublet content of the unperturbed states. The rate of the reaction will depend on the recombination rate of the singlet exciton and the intraexciton and exciton-polaron exchange strengths,

$$r_{\text{exciton-polaron}} = r_{\text{singlet}}\frac{\Delta J_{ex,p}}{J_{ex}}, \tag{59}$$

where $r_{\text{exciton-polaron}}$ is the recombination rate of an exciton-polaron complex and r_{singlet} is the recombination rate of a singlet exciton. Since the singlet admixture will be proportional to the doublet content it provides the same dynamics as a process mediated directly via doublet content. A similar argument can be made involving recombination due to a slightly asymmetric dipolar coupling between the exciton and polaron.

VI. CONCLUSION

Triplet-exciton polaron quenching plays an important role in the large magnetic field effects observed in organic semiconductors. We have developed a general time-domain theory which quantitatively describes the changes in samples conductivity due to this mechanism in pulsed electrically detected magnetic resonance. Population mixing due to resonant excitation causes a net change in the exciton-polaron reaction rate, and hence the free polaron density.

In particular, we have derived transition frequencies and resonance positions for an exciton-polaron complex with arbitrary coupling. Our modeling indicates that there is a clearly discernible transition between an uncoupled exciton-polaron state and a strongly bound trion. These

states may be differentiated through their transition frequencies and resonance positions. Our formalism provides a general basis for quantitative analysis of the triplet-exciton polaron process through pEDMR. In the future multipulse schemes, such as the Hahn echo (T_2) or inversion recovery (T_1), could be used to investigate relaxation processes directly.

ACKNOWLEDGMENTS

This work was supported by the Australian Research Council (ARC) (Grants No. DP120102888 and No. CE110001027). T.L.K. is supported by the Australian Renewable Energy Agency (ARENA) (Grant No. 7-S009). D.R.M. acknowledges an Australian Research Council (ARC) Future Fellowship (No. FT130100214).

APPENDIX A: HAMILTONIAN

The exciton-polaron Hamiltonian from Eq. (9) can be expanded in the product basis, producing the matrix

$$\begin{bmatrix} \mathscr{H}_{11} & 0 & 0 & 0 & 0 & 0 \\ 0 & \frac{\omega}{2}+\frac{\omega_p}{2}-\frac{2D_{ex}}{3} & 0 & -\frac{\sqrt{2}D_{ex,p}}{6}-\frac{J_{ex,p}}{\sqrt{2}} & 0 & 0 \\ 0 & 0 & \frac{\omega}{2}+\frac{D_{ex}}{3}-\frac{D_{ex,p}}{3}+\frac{J_{ex,p}}{2}+\frac{\omega_p}{2}-\omega_{ex} & 0 & -\frac{\sqrt{2}D_{ex,p}}{6}-\frac{J_{ex,p}}{\sqrt{2}} & 0 \\ 0 & -\frac{\sqrt{2}D_{ex,p}}{6}-\frac{J_{ex,p}}{\sqrt{2}} & 0 & -\frac{\omega}{2}+\frac{D_{ex}}{3}-\frac{D_{ex,p}}{3}+\frac{J_{ex,p}}{2}-\frac{\omega_p}{2}+\omega_{ex} & 0 & 0 \\ 0 & 0 & -\frac{\sqrt{2}D_{ex,p}}{6}-\frac{J_{ex,p}}{\sqrt{2}} & 0 & -\frac{\omega}{2}-\frac{2D_{ex}}{3}-\frac{\omega_p}{2} & 0 \\ 0 & 0 & 0 & 0 & 0 & \mathscr{H}_{66} \end{bmatrix}, \tag{A1}$$

where $\mathscr{H}_{11}=\frac{3\omega}{2}+\frac{D_{ex}}{3}+\frac{D_{ex,p}}{3}-\frac{J_{ex}}{2}+\frac{\omega_o}{2}+\omega_{ex}$ and $H_{66}=-\frac{3\omega}{2}+\frac{D_{ex}}{3}+\frac{D_{ex,p}}{3}-\frac{J_{ex}}{2}-\frac{\omega_p}{2}-\omega_{ex}$.

The static Hamiltonian ($\mathscr{H}_0$) may be transformed to the energy eigenbasis using the unitary matrix from Eq. (11),

$$E_1=\frac{3\omega}{2}+\frac{D_{ex}}{3}+\frac{D_{ex,p}}{3}-\frac{J_{ex}}{2}+\frac{\omega_p}{2}+\omega_{ex}, \tag{A2}$$

$$E_2=\frac{\omega}{2}+\frac{J_{ex}}{4}-\frac{D_{ex,p}}{6}-\frac{D_{ex}}{6}-\frac{\omega_{ex}}{2}-\left(\frac{1}{3}(6D_{ex}-2D_{ex,p}+3J_{ex})^2+\frac{8}{3}(D_{ex,p}+3J_{ex})^2\right), \tag{A3}$$

$$E_3=\frac{\omega}{2}+\frac{J_{ex}}{4}-\frac{D_{ex,p}}{6}-\frac{D_{ex}}{6}-\frac{\omega_{ex}}{2}+\left(\frac{1}{3}(6D_{ex}-2D_{ex,p}+3J_{ex})^2+\frac{8}{3}(D_{ex,p}+3J_{ex})^2\right), \tag{A4}$$

$$E_4=-\frac{\omega}{2}+\frac{J_{ex}}{4}-\frac{D_{ex,p}}{6}-\frac{D_{ex}}{6}+\frac{\omega_{ex}}{2}+\left(\frac{1}{3}(6D_{ex}-2D_{ex,p}+3J_{ex})^2+\frac{8}{3}(D_{ex,p}+3J_{ex})^2\right), \tag{A5}$$

$$E_5=-\frac{\omega}{2}+\frac{J_{ex}}{4}-\frac{D_{ex,p}}{6}-\frac{D_{ex}}{6}+\frac{\omega_{ex}}{2}-\left(\frac{1}{3}(6D_{ex}-2D_{ex,p}+3J_{ex,p})^2+\frac{8}{3}(D_{ex,p}+3J_{ex})^2\right), \tag{A6}$$

$$E_6=-\frac{3\omega}{2}+\frac{D_{ex}}{3}+\frac{D_{ex,p}}{3}-\frac{J_{ex}}{2}-\frac{\omega_p}{2}-\omega_{ex}. \tag{A7}$$

The first and last matrix elements form 1×1 subspaces in the product basis and are left unaffected by diagonalization. The perturbative $\mathscr{H}_1$ driving terms are strictly off-diagonal elements, which mix the eigenstates, and determine the transition frequencies:

$$B_{12}=B_{21}=\frac{B_1}{2}(\sin\theta+\sqrt{2}\cos\theta), \tag{A8}$$

$$B_{14}=B_{41}=\frac{B_1}{2}(\cos\theta-\sqrt{2}\sin\theta), \tag{A9}$$

$$B_{23}=B_{32}=-\frac{B_1}{2}(\cos\theta\sin\phi-\sqrt{2}\cos\theta\cos\phi+\sqrt{2}\sin\theta\sin\phi), \tag{A10}$$

$$B_{25}=B_{52}=\frac{B_1}{2}(\cos\theta\cos\phi+\sqrt{2}\cos\theta\sin\phi+\sqrt{2}\sin\theta\cos\phi), \tag{A11}$$

$$B_{34}=B_{43}=-\frac{B_1}{2}(\sqrt{2}\cos\theta\sin\phi-\sin\theta\sin\phi+\sqrt{2}\cos\phi\sin\theta), \tag{A12}$$

$$B_{36}=B_{63}=\frac{B_1}{2}(\cos\phi-\sqrt{2}\sin\phi), \tag{A13}$$

$$B_{45}=B_{54}=-\frac{B_1}{2}(\cos\theta\cos\phi-\sqrt{2}\cos\theta\sin\phi+\sqrt{2}\sin\theta\sin\phi), \tag{A14}$$

$$B_{56}=B_{65}=\frac{B_1}{2}(\sin\phi+\sqrt{2}\cos\phi). \tag{A15}$$

Substitution of these expressions into Eq. (28) provides a general description of the coherent dynamics of an exciton-polaron complex.

APPENDIX B: RESONANCE POSITION

The resonance positions are given by the energy differences of the eigenstates,

$$\omega_{ij} = E_i - E_j. \tag{B1}$$

These are calculated explicitly from Eqs. (A2)–(A7) and given in Table III. All of the transitions have a resonance position which depends on the spin coupling term X, which indicates that all of the transitions will become very broad as the exciton-polaron coupling becomes large.

TABLE III. Resonance positions for an exciton polaron with arbitrary spin-spin coupling, calculated from Eqs. (A2)–(A7). In the table below $X = [\frac{1}{3}(6D_{ex} - 2D_{ex,p} + 3J_{ex,p})^2 + \frac{8}{3}(D_{ex,p} + 3J_{ex,p})^2]$.

Transition	ΔE
(1)-(2)	$\frac{D_{ex}}{2} + \frac{D_{ex,p}}{2} - \frac{3J_{ex,p}}{4} + \frac{\omega_p}{2} + \frac{\omega_{ex}}{2} + X$
(1)-(4)	$\frac{D_{ex}}{2} + \frac{D_{ex,p}}{2} - \frac{3J_{ex,p}}{4} + \frac{\omega_p}{2} + \frac{\omega_{ex}}{2} - X$
(2)-(3)	$\omega_{ex} - 2X$
(2)-(5)	ω_{ex}
(3)-(4)	ω_{ex}
(3)-(6)	$\frac{3J_{ex,p}}{4} - \frac{D_{ex,p}}{2} - \frac{D_{ex}}{2} + \frac{\omega_p}{2} + \frac{\omega_{ex}}{2} + X$
(4)-(5)	$\omega_{ex} + 2X$
(5)-(6)	$\frac{3J_{ex,p}}{4} - \frac{D_{ex,p}}{2} - \frac{D_{ex}}{2} + \frac{\omega_{ex}}{2} - X$

APPENDIX C: MICROSCOPIC BASIS FOR RECOMBINATION

The expanded (antisymmetric) exchange matrix can be expanded using the standard tensor product [43] and is

$$\begin{bmatrix} 0 & 0 & 0 & 0 & 0 & 0 & 0 & 0 \\ 0 & 0 & \frac{\Delta J_{ex,p}}{2} & 0 & -\frac{\Delta J_{ex,p}}{\sqrt{2}} & 0 & 0 & 0 \\ 0 & \frac{\Delta J_{ex,p}}{2} & 0 & 0 & 0 & 0 & 0 & 0 \\ 0 & 0 & 0 & 0 & 0 & \frac{\Delta J_{ex,p}}{\sqrt{2}} & 0 & 0 \\ 0 & -\frac{\Delta J_{ex,p}}{\sqrt{2}} & 0 & 0 & 0 & 0 & 0 & 0 \\ 0 & 0 & 0 & \frac{\Delta J_{ex,p}}{\sqrt{2}} & 0 & 0 & -\frac{\Delta J_{ex,p}}{2} & 0 \\ 0 & 0 & 0 & 0 & 0 & -\frac{\Delta J_{ex,p}}{2} & 0 & 0 \\ 0 & 0 & 0 & 0 & 0 & 0 & 0 & 0 \end{bmatrix}, \tag{C1}$$

where the coupling term is written in the expanded singlet/triplet-doublet basis. All of the matrix elements lie on off-diagonal elements, which means the first order effect will be to slightly admix the eigenstates, but not change the energies. This term therefore allows the canonical triplet-doublet states to project onto the singlet-doublet states. A similar argument can be made for the exciton-polaron dipolar coupling term.

[1] T. Francis, Ö. Mermer, G. Veeraraghavan, and M. Wohlgenannt, New J. Phys. **6**, 185 (2004).

[2] Ö. Mermer, G. Veeraraghavan, T. L. Francis, Y. Sheng, D. T. Nguyen, M. Wohlgenannt, A. Köhler, M. K. Al-Suti, and M. S. Khan, Phys. Rev. B **72**, 205202 (2005).

[3] R. Mahato, H. Lülf, M. Siekman, S. Kersten, P. Bobbert, M. de Jong, L. De Cola, and W. van der Wiel, Science **341**, 257 (2013).

[4] H. Hoppe and N. S. Sariciftci, J. Mater. Res. **19**, 1924 (2004).

[5] A. Dodabalapur, Solid State Commun. **102**, 259 (1997).

[6] W. J. Baker, K. Ambal, D. Waters, R. Baarda, H. Morishita, K. van Schooten, D. R. McCamey, J. M. Lupton, and C. Boehme, Nat. Commun. **3**, 898 (2012).

[7] V. Prigodin, J. Bergeson, D. Lincoln, and A. Epstein, Synth. Met. **156**, 757 (2006).

[8] P. Desai, P. Shakya, T. Kreouzis, and W. P. Gillin, Phys. Rev. B **76**, 235202 (2007).

[9] P. A. Bobbert, T. D. Nguyen, F. W. A. van Oost, B. Koopmans, and M. Wohlgenannt, Phys. Rev. Lett. **99**, 216801 (2007).

[10] P. Janssen, M. Cox, S. Wouters, M. Kemerink, M. Wienk, and B. Koopmans, Nat. Commun. **4**, 2286 (2013).

[11] C. Boehme and J. M. Lupton, Nat. Nanotechnol. **8**, 612 (2013).

[12] C. Boehme and K. Lips, Phys. Rev. B **68**, 245105 (2003).

[13] T. L. Keevers, A. Danos, T. W. Schmidt, and D. R. McCamey, Nat. Nanotechnol. **8**, 886 (2013).

[14] A. Schweiger and G. Jeschke, *Principles of Pulse Electron Paramagnetic Resonance* (Oxford University Press, Oxford, 2001).

[15] D. R. McCamey, K. J. van Schooten, W. J. Baker, S.-Y. Lee, S.-Y. Paik, J. M. Lupton, and C. Boehme, Phys. Rev. Lett. **104**, 017601 (2010).

[16] W. J. Baker, T. L. Keevers, J. M. Lupton, D. R. McCamey, and C. Boehme, Phys. Rev. Lett. **108**, 267601 (2012).

[17] D. R. McCamey, H. Seipel, S. Paik, M. Walter, N. Borys, J. Lupton, and C. Boehme, Nat. Mater. **7**, 723 (2008).

[18] D. R. McCamey, S.-Y. Lee, S.-Y. Paik, J. M. Lupton, and C. Boehme, Phys. Rev. B **82**, 125206 (2010).

[19] H. Malissa, M. Kavand, D. Waters, K. van Schooten, P. Burn, Z. Vardeny, B. Saam, J. Lupton, and C. Boehme, Science **345**, 1487 (2014).
[20] F. Hoehne, L. Dreher, J. Behrends, M. Fehr, H. Huebl, K. Lips, A. Schnegg, M. Suckert, M. Stutzmann, and M. S. Brandt, Rev. Sci. Instrum. **83**, 043907 (2012).
[21] T. D. Nguyen, B. R. Gautam, E. Ehrenfreund, and Z. V. Vardeny, Phys. Rev. Lett. **105**, 166804 (2010).
[22] A. J. Schellekens, W. Wagemans, S. P. Kersten, P. A. Bobbert, and B. Koopmans, Phys. Rev. B **84**, 075204 (2011).
[23] V. Rajevac, C. Boehme, C. Michel, A. Gliesche, K. Lips, S. D. Baranovskii, and P. Thomas, Phys. Rev. B **74**, 245206 (2006).
[24] A. Gliesche, C. Michel, V. Rajevac, K. Lips, S. D. Baranovskii, F. Gebhard, and C. Boehme, Phys. Rev. B **77**, 245206 (2008).
[25] M. E. Limes, J. Wang, W. J. Baker, S.-Y. Lee, B. Saam, and C. Boehme, Phys. Rev. B **87**, 165204 (2013).
[26] J. Shinar, Laser Photon. Rev. **6**, 767 (2012).
[27] K. J. van Schooten, C. Boehme, and J. M. Lupton, ChemPhysChem **15**, 1737 (2014).
[28] A. Belolipetskiy, O. Gusev, A. Dmitriev, E. Terukov, and I. Yassievich, Semiconductors **48**, 235 (2014).
[29] S. Weber, G. Kothe, and J. R. Norris, J. Chem. Phys. **106**, 6248 (1997).
[30] J. Y. Song, N. Stingelin, A. J. Drew, T. Kreouzis, and W. P. Gillin, Phys. Rev. B **82**, 085205 (2010).
[31] M. Cox, P. Janssen, F. Zhu, and B. Koopmans, Phys. Rev. B **88**, 035202 (2013).
[32] M. A. Baldo and S. R. Forrest, Phys. Rev. B **62**, 10958 (2000).
[33] W. J. Baker, D. R. McCamey, K. J. van Schooten, J. M. Lupton, and C. Boehme, Phys. Rev. B **84**, 165205 (2011).
[34] V. Ern and R. Merrifield, Phys. Rev. Lett. **21**, 609 (1968).
[35] W. J. Baker, T. L. Keevers, C. Boehme, and D. R. McCamey, arXiv:1502.05471.
[36] H. Huebl, F. Hoehne, B. Grolik, A. R. Stegner, M. Stutzmann, and M. S. Brandt, Phys. Rev. Lett. **100**, 177602 (2008).
[37] S. Stafström, Chem. Soc. Rev. **39**, 2484 (2010).
[38] F. L. Bloom, M. Kemerink, W. Wagemans, and B. Koopmans, Phys. Rev. Lett. **103**, 066601 (2009).
[39] A. G. Redfield, IBM J. Res. Dev. **1**, 19 (1957).
[40] N. Atherton, *Principles of Electron Paramagnetic Resonance* (Ellis Horwood Limited, Chichester, England, 1993).
[41] C. Deibel and V. Dyakonov, Rep. Prog. Phys. **73**, 096401 (2010).
[42] Y. Kandrashkin and A. van der Est, J. Chem. Phys **120**, 4790 (2004).
[43] J. J. Sakurai and S. F. Tuan, *Modern Quantum Mechanics* (Addison-Wesley, Reading, MA, 1994), Vol. 104.
[44] M. Asano-Someda, A. van der Est, U. Krüger, D. Stehlik, Y. Kaizu, and H. Levanon, J. Phys. Chem. A **103**, 6704 (1999).
[45] Y. Kandrashkin and A. van der Est, Chem. Phys. Lett. **379**, 574 (2003).
[46] A. van der Est, M. Asano-Someda, P. Ragogna, and Y. Kaizu, J. Phys. Chem. A **106**, 8531 (2002).
[47] Y. Kobori, K. Takeda, K. Tsuji, A. Kawai, and K. Obi, J. Phys. Chem. A **102**, 5160 (1998).
[48] F. Hoehne, C. Huck, M. S. Brandt, and H. Huebl, Phys. Rev. B **89**, 161305 (2014).
[49] J.-L. Brédas, D. Beljonne, V. Coropceanu, and J. Cornil, Chem. Rev. **104**, 4971 (2004).